SOURCE FLOW EFFECTS IN CONICAL HYPERVELOCITY NOZZLES

By

Jack D. Whitfield and Glenn D. Norfleet
von Kármán Gas Dynamics Facility
ARO, Inc.,
a subsidiary of Sverdrup and Parcel, Inc.

June 1962

ARO Project No. 360213

AF - AEDC
Arnold AFS Tenn

ABSTRACT

Source flow effects in conical hypervelocity nozzles are studied by means of a simple Newtonian theory for slender conical bodies. Experiments were conducted to examine the validity of this simple theoretical approach and a semiempirical theory is developed to assess the magnitude of source flow effects. Significant source flow effects were found, and the need for contoured hypervelocity wind tunnel nozzles is shown.

CONTENTS

ILLUSTRATIONS

NOMENCLATURE

C_D	Zero-lift drag coefficient, based on base area
ΔC_D	Change in drag coefficient caused by source flow
D	Model base diameter
d_N	Model nose diameter
K	Empirical constant (see Eq. (11))
ℓ	Model length to point considered (see Fig. 3)
ℓ_N	Nozzle length (see Fig. 3)
M	Free-stream Mach number
p_c	Cone pressure
Δp_c	Change in cone pressure caused by source flow
p_o	Total stagnation pressure
p_o'	Pitot pressure at model nose
p_w	Model surface pressure
p_∞	Free-stream static pressure
q_∞	Free-stream dynamic pressure at model nose
Δq	Change in dynamic pressure caused by source flow
R	Local wind tunnel nozzle radius
Re/in.	Free-stream Reynolds number per inch
r	Local model radius
r_B	Model base radius
r_N	Model nose radius
T_o	Total stagnation temperature
x	Distance along model surface (see Fig. 3)
y	Distance from nozzle centerline to model pressure orifice (see Fig. 5)
ϵ	Local flow angularity caused by source flow
θ_c	Cone half-vertex angle
θ_N	Nozzle half-vertex angle

ξ	r_N/r_B (nose bluntness ratio)
ρ_o	Arc-chamber density in amagat units where 1 amagat is the density at one standard atmosphere pressure at 273.16°K (for nitrogen: 1 amagat = 2.424×10^{-3} lb-sec^2/ft^4
ρ_∞	Free-stream density in amagat units
$( )_s$	In source flow

1.0 INTRODUCTION

It has been a general practice in the past to use simple, conical nozzles for hypervelocity tunnels, whether of the shock or hotshot type. This was done for both economic and technical reasons. It was cheap and convenient to vary the Mach number over wide ranges by changing only the throat size. Also, suitable methods of calculation of boundary layers in hypervelocity nozzle flow have not been developed. Thus, conical nozzles have been widely used because they have a sufficient divergence to prevent excessive boundary-layer growth and yet small enough to attempt to produce acceptable axial density gradients and radial flow angularity effects. The 10-deg and 8-deg total angle conical nozzles of the hypervelocity tunnels of the von Kármán Gas Dynamics Facility, Arnold Engineering Development Center (VKF-AEDC), Air Force Systems Command (AFSC), are examples of such a compromise.

Improvements in the precision of measurements in hypervelocity tunnels have led to the realization that the flow divergence in conical nozzles may, under some circumstances, cause serious errors. An analytical estimate of these effects on the inviscid pressure distributions and total drag of slender cones is given in Ref. 1. Burke and Bird (Ref. 2) also treated this problem and arrived at similar conclusions.

Although in practice the contouring effect of the nozzle boundary layer may reduce the radial flow effects in conical nozzles (cf, e.g., Ref. 3), this must be established in each specific case. It is the purpose of this report to present measurements in support of the simple analysis given in Ref. 1 and to document these effects in the present AEDC-VKF hypervelocity conical nozzles.

2.0 TEST APPARATUS

The new experimental data reported herein were obtained from the VKF-AEDC, 50-Inch Hypervelocity Tunnel (Hotshot 2) (Fig. 1) described in Ref. 1. The tests were performed with nitrogen as a test gas at a nominal stagnation temperature and pressure of 3300°K and 13,000 psia, respectively. Typical test conditions are given below.

M	Re/in.	p_o, psia	T_o, °K	p'_o, psia	p_∞, psia	ρ_∞, amagat units
19.2	20,600	13,250	3320	1.08	0.0023	0.00079

Manuscript released by authors May 1962.

Surface pressures were obtained at various locations on the models as shown in Fig. 2. The pressures were measured with wafer-style pressure transducers as discussed in Ref. 1. A pitot pressure measurement was obtained during each tunnel run, either from a total head probe in the model nose or from a separate total head probe aligned longitudinally with the model nose.

3.0 PRECISION OF MEASUREMENTS

The accuracy of results from any high temperature hypersonic test facility is, of course, a function not only of the uncertainty of the direct measurements, but also of the validity of the assumptions and the gas properties used in inferring the flow conditions. For example, it has recently been shown in Ref. 1 that the conventional method used in hot-shot wind tunnels for arriving at the enthalpy of the test gas by using the measured arc-chamber pressure and an initial knowledge of the gas density is likely to contain appreciable error. Fortunately, the tests reported herein were relatively insensitive to this effect since this study is concerned with inviscid surface pressures. It can be shown that the normalizing of measured inviscid surface pressures by the measured pitot pressure (hence dynamic pressure) produces a ratio which is insensitive to Mach number and Reynolds number (and hence enthalpy) per se.

In general, the uncertainty of bench calibrations of the pressure transducers was approximately ±2 percent, whereas the repeatability of such measurements, as indicated by repeated tunnel runs, was approximately ±5 percent.

4.0 THEORY-NEWTONIAN AND SOURCE FLOW

The proper parametric form and the upper limits of radial flow effects can be studied by assuming a pure conical source flow over simple bodies. A slender conical body shape is assumed here for simplicity.

4.1 INVISCID LOCAL CONE PRESSURES

Newtonian pressure, given approximately (for $\sin^2 \theta_c \sim \theta_c^2$ and $p_c >> p_\infty$) by

$$\frac{p_c}{q_\infty} \approx 2\,\theta_c^2 \qquad (1)$$

is used here to estimate the source flow effects. Considering the nomenclature of Fig. 3, then the local cone pressure in a source flow may be written as

$$(p_c)_s \approx 2(\theta_c - \epsilon)^2 (q_\infty + \Delta q) \tag{2}$$

where q_∞ is taken at the model nose and Δq is the change in dynamic pressure from the nose to the point considered. Neglecting second-order terms, this equation may be expanded to give

$$(p_c)_s \approx 2\,\theta_c^2\, q_\infty \left[1 - 2\,\frac{\epsilon}{\theta_c} + \frac{\Delta q}{q_\infty}\right] \tag{3}$$

or

$$\frac{(p_c)_s}{2\theta_c^2\, q_\infty} = 1 - 2\,\frac{\epsilon}{\theta_c} + \frac{\Delta q}{q_\infty} \tag{3a}$$

Thus

$$\frac{\Delta p_c}{p_c} \approx -2\,\frac{\epsilon}{\theta_c} + \frac{\Delta q}{q_\infty} \tag{4}$$

It should be noted that these terms are additive since Δq will be negative in a diverging supersonic flow. The ϵ/θ_c term may be written directly from the geometry noted in Fig. 3,

$$\frac{\epsilon}{\theta_c} = \left(\frac{r}{R}\right)\left(\frac{\theta_N}{\theta_c}\right) \tag{5}$$

The $\Delta q/q_\infty$ term may be evaluated by noting that for $M >> 1$

$$q \propto A^*/A \propto 1/\ell_N^2 \tag{6}$$

Therefore

$$\frac{\Delta q}{q_\infty} = -2\,\frac{\ell}{\ell_N} = -2\left(\frac{r}{R}\right)\left(\frac{\theta_N}{\theta_c}\right) \tag{7}$$

The flow angularity effect and the dynamic pressure gradient effect are equal and additive. The total error in cone pressure is

$$\frac{\Delta p_c}{p_c} = -4\left(\frac{r}{R}\right)\left(\frac{\theta_N}{\theta_c}\right) \tag{8}$$

4.2 INVISCID CONE DRAG

The source flow effect on total inviscid cone drag may be readily obtained from the above expressions for local cone pressures. The cone drag in source flow is

$$(C_D)_s = \frac{2\int_o^{r_B} (p_c)_s \, r\,dr}{q_\infty \, r_B^2} \tag{9}$$

where again the reference station, ∞, is taken at the model nose. By substituting Eq. (3) and integrating and normalizing the drag error by the drag coefficient in uniform parallel flow, the following expression is obtained:

$$\frac{\Delta C_D}{C_D} = \frac{2}{3}\left(\frac{\Delta p_c}{p_c}\right)_{r_B} = -\frac{8}{3}\left(\frac{r_B}{R}\right)\left(\frac{\theta_N}{\theta_c}\right) \tag{10}$$

The magnitude of effects estimated from the above equations should represent the limiting case with a negligible contouring effect from the nozzle boundary layer, provided the Newtonian approximation indicates the correct pressure level. It will be shown later that the Newtonian approximation underestimates the pressure level for pure cones, and hence the limiting effects of source flow will be larger than indicated by the above equations.

5.0 COMPARISON OF THEORY AND EXPERIMENT

Equation (3a) indicates that in the case of pure source flow the local cone pressures should correlate with the parameter $\left[1 - (2\epsilon/\theta_c) + \Delta q/q_\infty\right]$ where this parameter is evaluated purely from geometric considerations. It should be noted that in the usual case with a model mounted on the wind tunnel axis, the flow angularity effect (represented by the $-2\epsilon/\theta_c$ term) and the axial density gradient effect (represented by the $\Delta q/q_\infty$ term) are equal and additive. By moving the test model off the tunnel axis and thus increasing the angularity term without changing the axial density gradient term, the relative magnitude of each of these terms, as well as their combined effect, can be studied.

The models originally tested by Lewis (Ref. 4) in Hotshot 1, the 16-inch hypervelocity tunnel, and a sharp 10-deg half-vertex angle cone were selected to experimentally study the source flow effects. The 9-deg cone models (Fig. 2) were included in this work in order to evaluate,

experimentally, the errors caused by source flow effects in the pressure distributions published in Ref. 4.

A summary plot of the measured sharp ($\xi \leq 0.03$) cone pressure data is presented as a function of the parameter $\left[1 - (2\epsilon/\theta_c) + \Delta q/q_\infty\right]$ in Fig. 4. The Newtonian source flow theory as computed directly from the theory outlined above is observed to be appreciably below the data. The curve labeled "73 percent Source Flow" represents a fairing through the experimental data, and the intersection of this curve with the abscissa value of one (i. e., $\epsilon = \Delta q = 0$) was taken as the correct or parallel flow value. The corrected Newtonian source flow theory was then computed using this corrected pressure level. It should be emphasized here that the data points presented are based only on measurement and the nozzle and model geometries. All of the "corrections" referred to above were applied only to the theory.

Using the corrected pressure level and the experimental fairing from Fig. 4, a semiempirical theoretical correction may be obtained for local cone pressures. This semiempirical theory is

$$\frac{(p_c)_s}{2\,\theta_c^2\,q_\infty} = 1.32\left[1 - 2K\,\frac{\epsilon}{\theta_c} + K\,\frac{\Delta q}{q_\infty}\right] \qquad (11)$$

where K is an empirical constant between zero and one representing the approach to pure inviscid source flow. In the specific cases studied here (i. e., the 16-in. and 50-in. AEDC-VKF hypervelocity tunnels), $K \approx 0.73$. For larger nozzle divergence angles it is expected that K would approach one. Illustrations of this semiempirical theory and of the magnitude of the source flow effects are shown in Fig. 5. The intercept values of the ordinate represent the effect caused by axial density gradients, and the slope of these curves represents the flow angularity effects. It is concluded that the simple theoretical model used herein illustrates the proper relative magnitude of the axial density gradient and flow angularity effects.

The total drag error for a sharp cone may be easily estimated from this semiempirical theory. Substitution of Eq. (11) into Eq. (9) and integrating and normalizing the drag error by the drag coefficient in uniform parallel flow yields

$$\frac{\Delta C_D}{C_D} = \frac{2}{3}\left[-2K\,\frac{\epsilon}{\theta_c} + K\,\frac{\Delta q}{q_\infty}\right] \qquad (12)$$

Equations (11) and (12) may be used to estimate the expected errors in a particular tunnel as a function of model size. An example for 9-deg

half-vertex angle cones in the three AEDC-VKF hypervelocity tunnels is shown in Fig. 6. Here it has been assumed that the nozzle boundary layer in the 100-in. tunnel will produce a contouring effect similar to that observed in the 16-in. and 50-in. tunnels (hence K = 0.73). It is evident from Fig. 6 that precision measurements on slender bodies in conical nozzles will require the use of models that are small in relation to tunnel size.

The development of the above semiempirical theory for source flow effects permits an estimate of magnitude of such errors in the sharper (ξ = 0.03) cone pressure distribution presented by Lewis (Ref. 4). The semiempirical theory developed here requires inviscid conical flow (i. e., $\partial p/\partial x = 0$), and such is clearly not the case in Lewis' data. The present measurements from the same model in a larger tunnel (50-in. hotshot) and the semiempirical theory are compared to Lewis' original measurement obtained from the 16-in. hotshot in Fig. 7. The estimated afterbody pressure level is observed to be nearly constant and above the perfect gas sharp cone value. The nose bluntness effect invalidates the correction theory near the nose, and hence an estimate of the influence of source flow on the overexpansion and recompression phenomena observed by Lewis cannot be accurately assessed.

The presence of large nose bluntness will significantly alter the influence of source flow effects. The Newtonian theory used for analysis of the sharp cone case requires the nose shock wave and body to be coincident, and, of course, large nose bluntness will produce a strong nose shock wave which invalidates this theoretical approach. In such a case the flow field may be dominated by the nose bluntness, and hence model surface conditions may be essentially determined by the free-stream conditions just upstream of the nose. An experimental check was made with the spherically blunted model (Fig. 2) which has an order of magnitude larger nose bluntness, ξ = 0.3. A comparison of the measured pressure distributions from this model in the 16-in. and the 50-in. tunnels is shown in Fig. 8. The large difference found for the sharper cone case was not observed, and the measurements agree within the uncertainty of the experiments. It is concluded that in this case the flow field is dominated by nose bluntness, and flow angularity and axial density gradient effects are quite markedly reduced.

6.0 CONCLUSIONS

Source flow effects are quite significant for slender, relatively sharp bodies. A semiempirical theory is developed for sharp cones to

estimate these effects as a function of cone angle, nozzle geometry, and degree of contouring effect from the nozzle boundary layer.

Source flow effects are shown to be markedly reduced in the presence of large nose bluntness. Thus, results from short, blunt bodies with high local flow deflections will be relatively unaffected by source flow effects.

Present and future hypervelocity testing demands increasing consideration of slender bodies. Source flow effects on slender bodies can be minimized by the use of models quite small with respect to wind tunnel size or, preferably, by the use of contoured hypervelocity nozzles. Thus, the necessity for the development of contoured, hypervelocity wind tunnel nozzles is evident.

REFERENCES

1. Lukasiewicz, J., Jackson, R., and Whitfield, J. D. "Status of Development of Hotshot Tunnels at the AEDC." Paper presented at the AGARD Meeting on "High Temperature Aspects of Hypersonic Flow", Training Center for Experimental Aerodynamics, Rhode-Saint-Genese, Belgium, April 3-6, 1962.

2. Burke, A. F. and Bird, K. D. "The Use of Conical and Contoured Expansion Nozzles in Hypervelocity Facilities." Paper presented at the Second National Symposium on Hypervelocity Techniques, Denver, Colorado, March 19 and 20, 1962 (CAL Report No. 112).

3. Johnson, R. H. "Hypersonic Viscous Effects in Wind Tunnels." ARS Journal, Vol. 31, No. 7, July 1961, pp 1022-1024.

4. Lewis, Clark H. "Pressure Distribution and Shock Shape Over Blunted Slender Cones at Mach Numbers from 16 to 19." AEDC-TN-61-81, August 1961.

5. General Electric Company. Private communications with H. Ridyard.

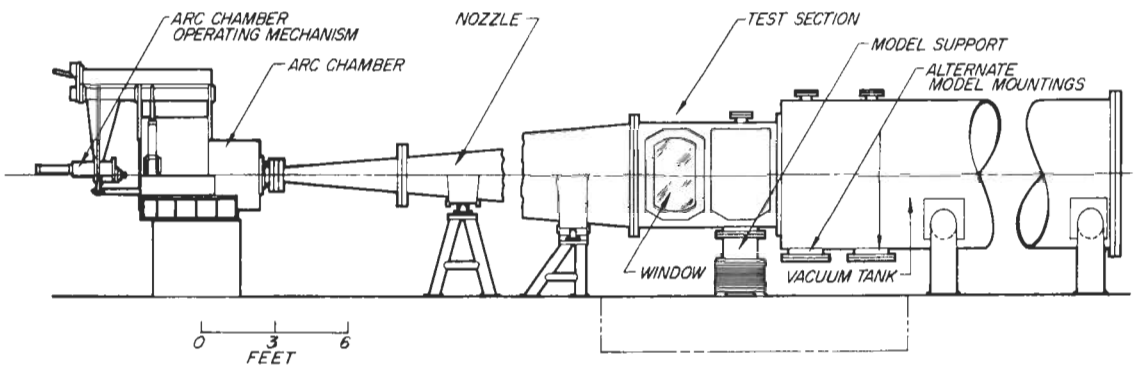

Assembly

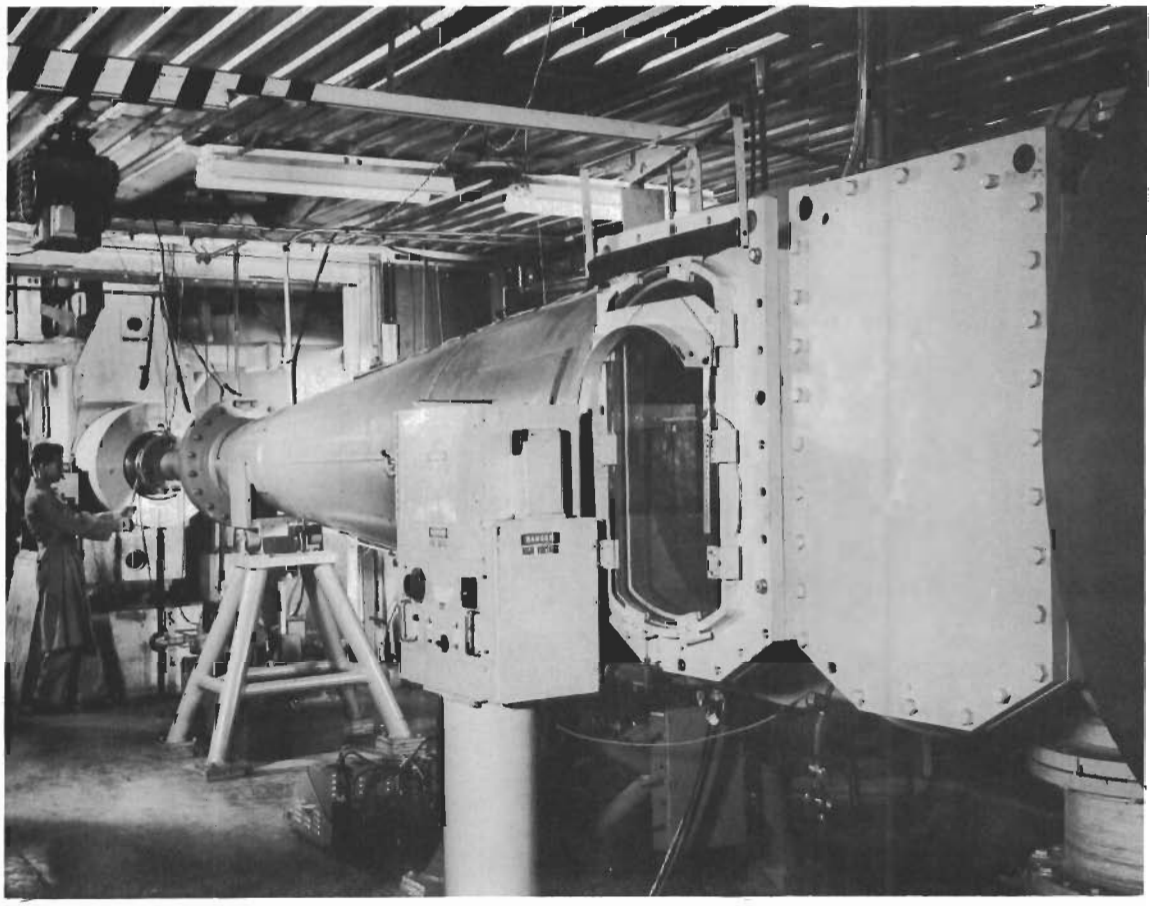

Arc Chamber, Nozzle, and Test Section

Fig. 1 The 50-Inch Hypervelocity Wind Tunnel (Hotshot 2)

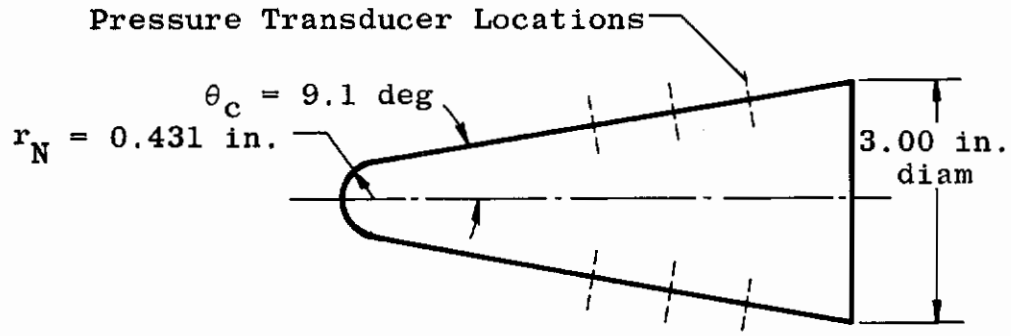

a. Spherically Blunted 9-Deg Cone

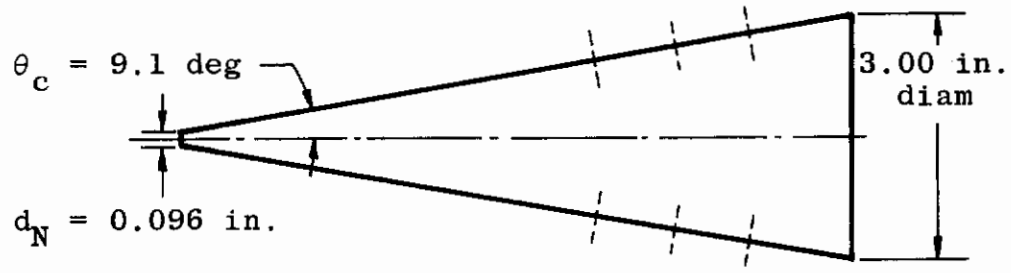

b. Flat-Nosed 9-Deg Cone

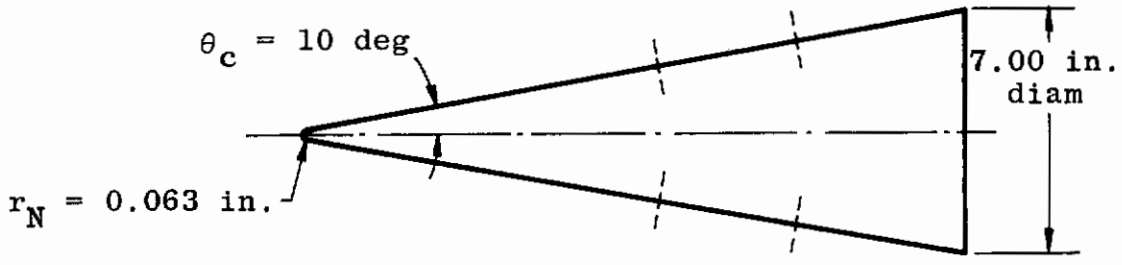

c. 10-Deg Cone

Fig. 2 Schematics of Models

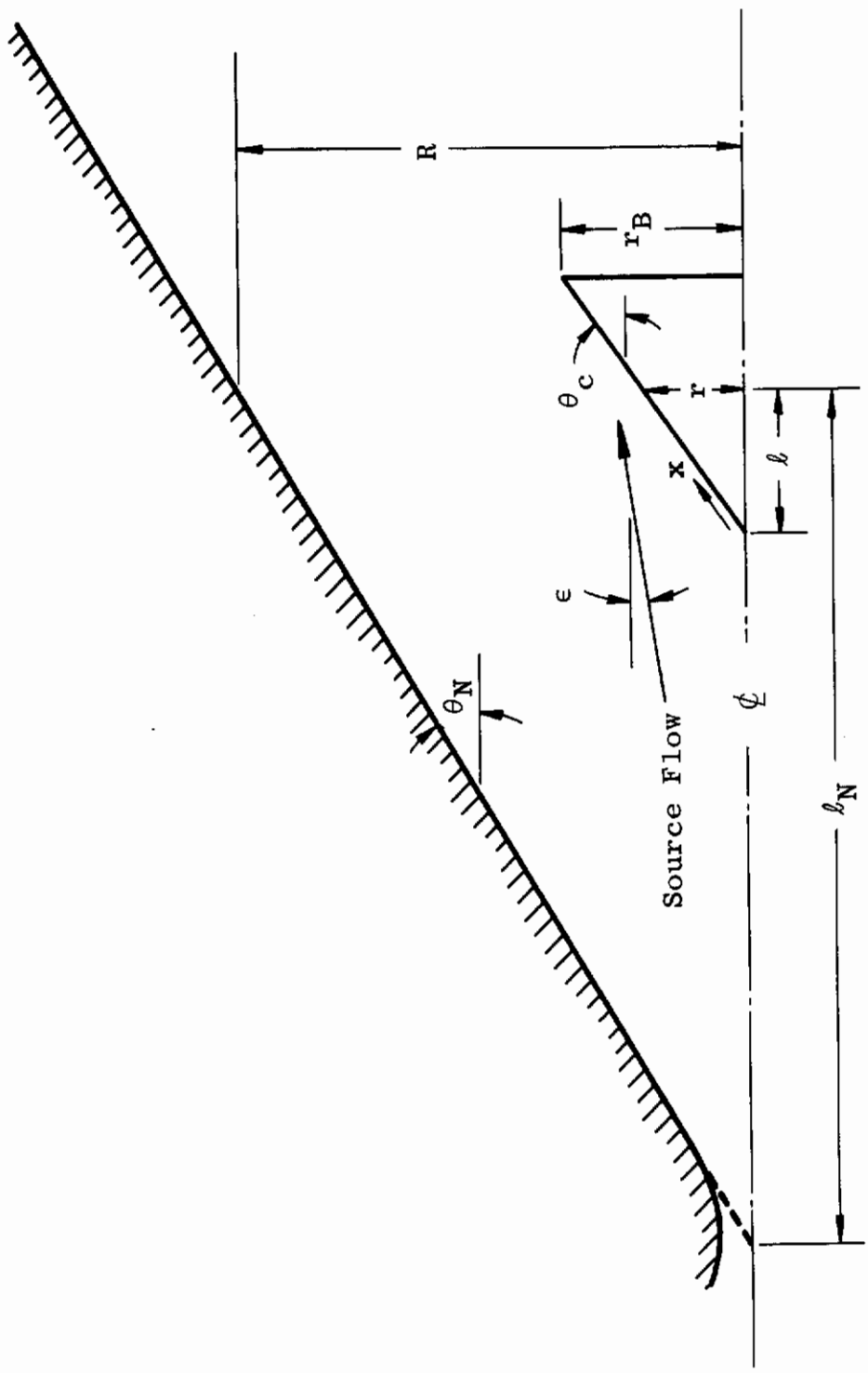

Fig. 3 Nomenclature Used for Derivation of Source Flow Effects on Cones

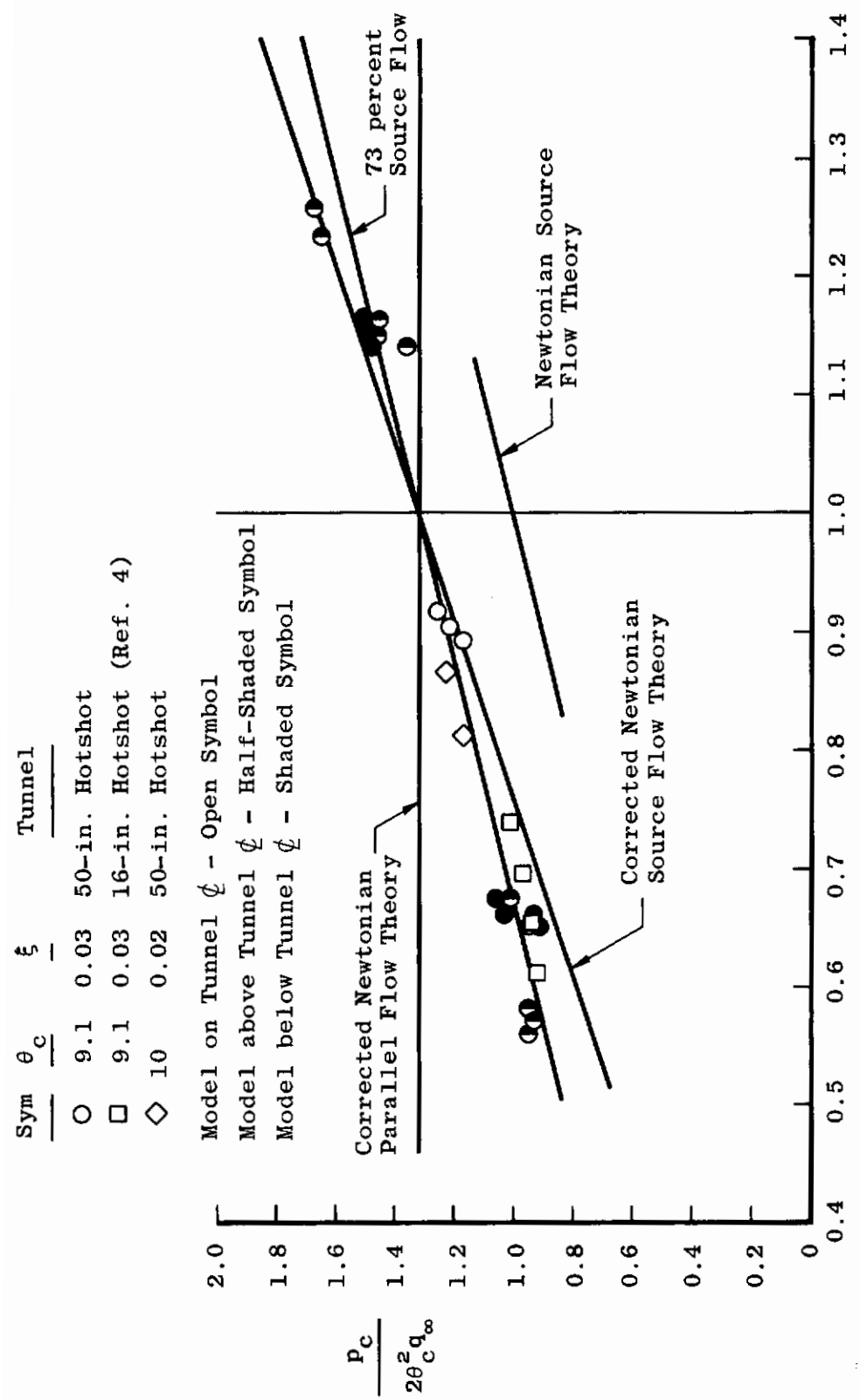

Fig. 4 Summary of Sharp Cone Pressure Data

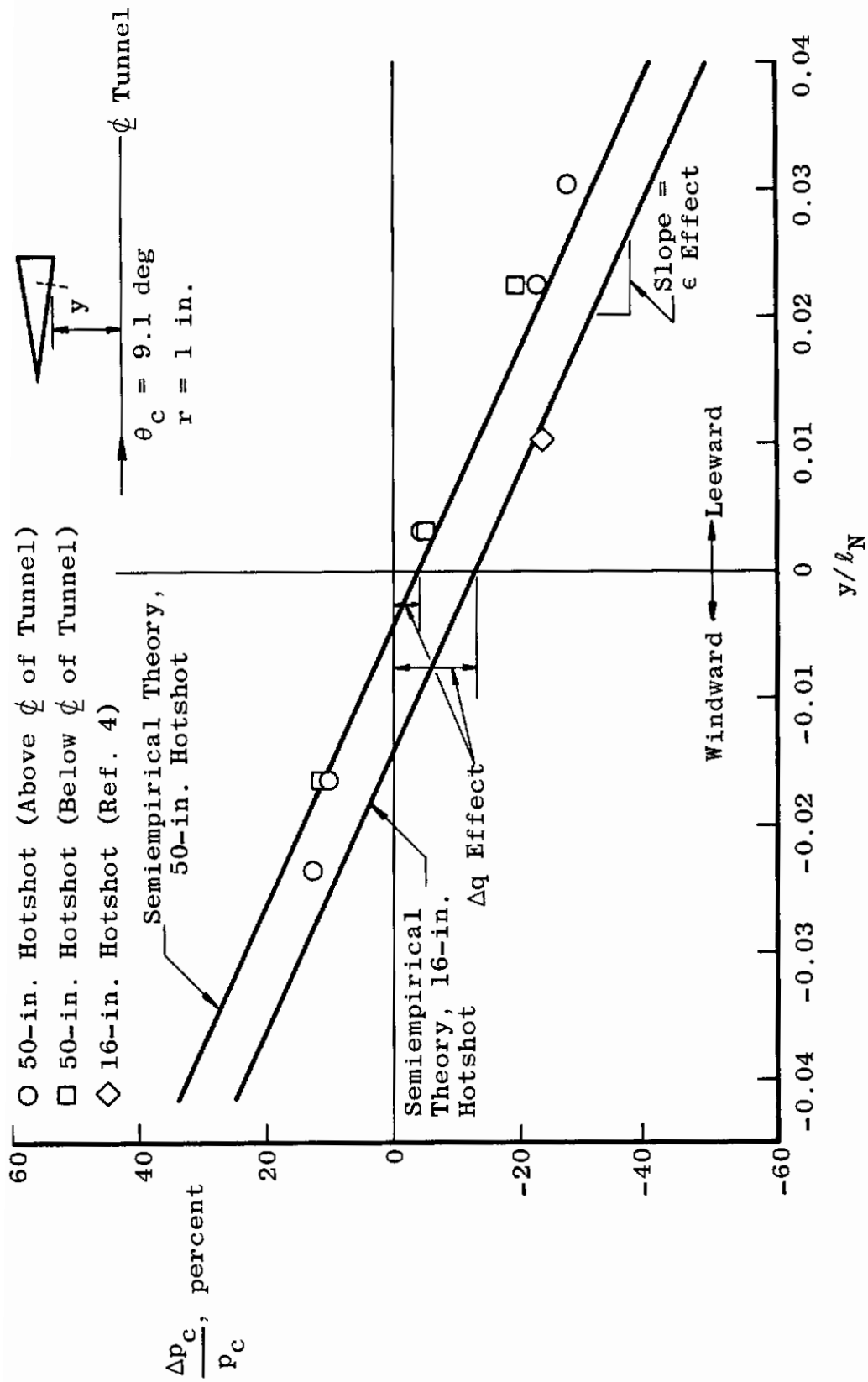

Fig. 5 Separation of Axial Density Gradient and Flow Angularity Effects

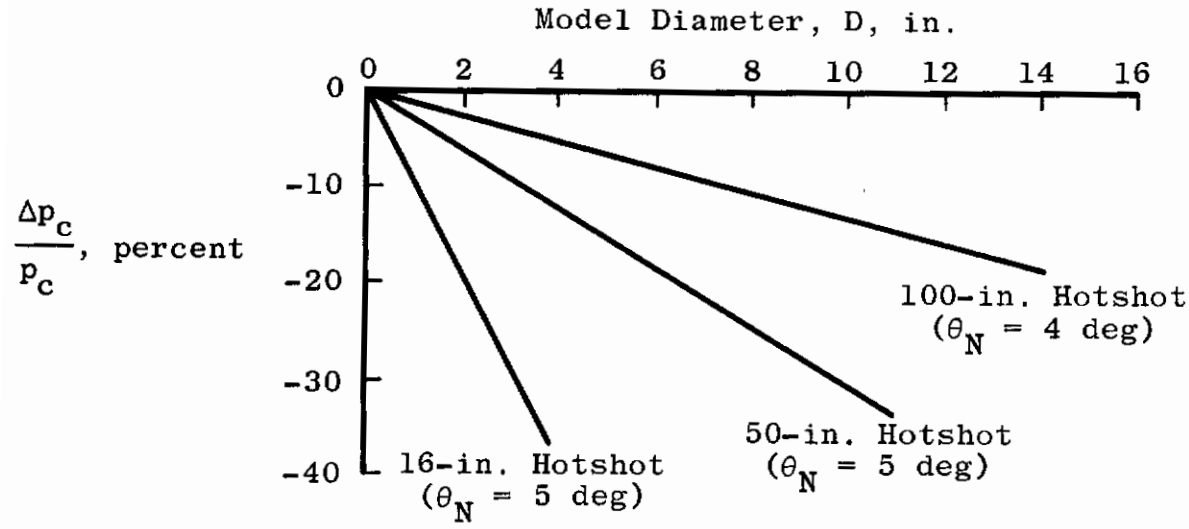

a. Local Cone Pressure Error

θ_c = 9 deg

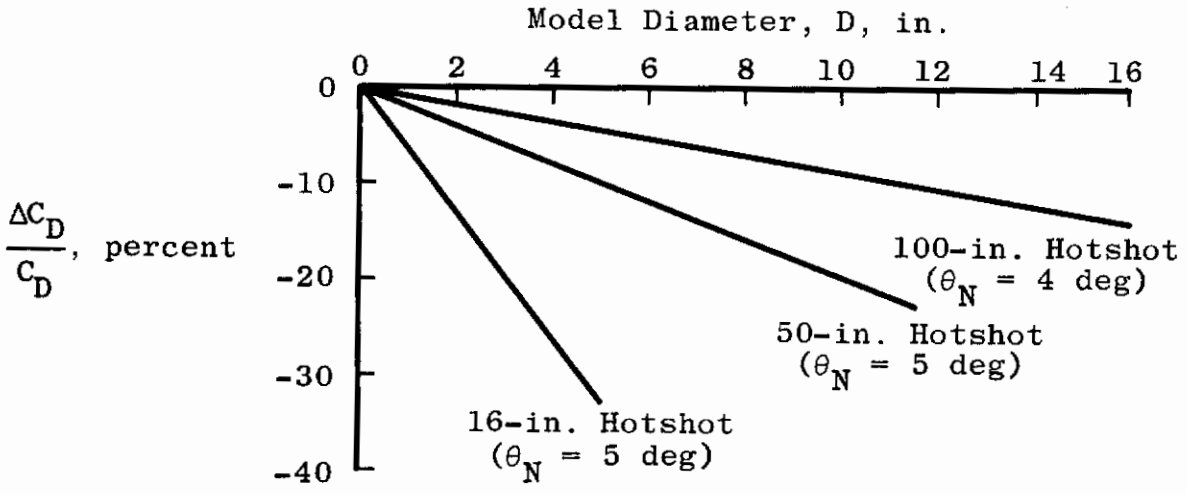

b. Cone Drag Error

Fig. 6 Source Flow Errors in Cone Pressure and Drag for 9-Deg Cones from Semiempirical Theory

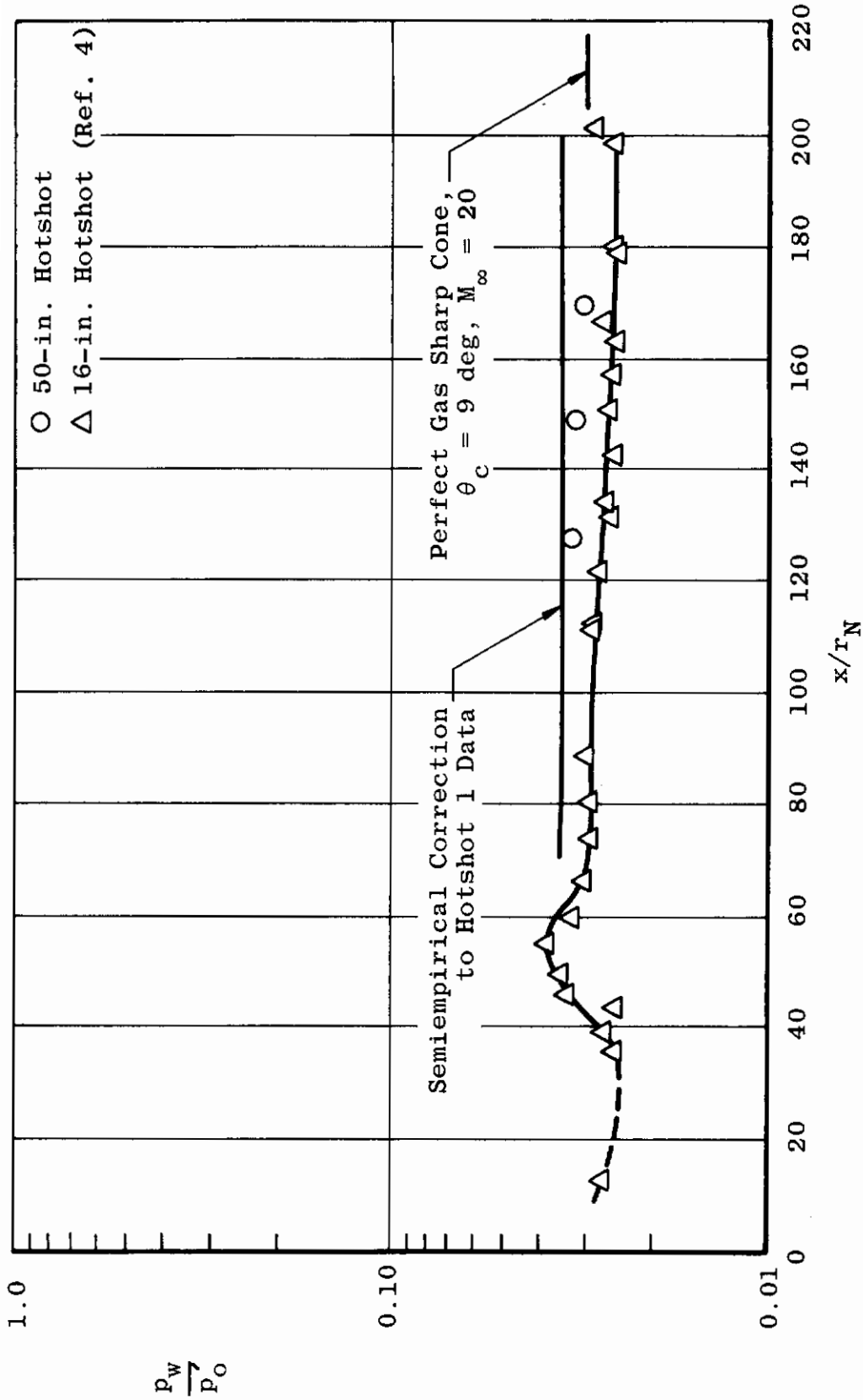

Fig. 7 Pressure Distribution, Flat-Nosed 9-Deg Cone

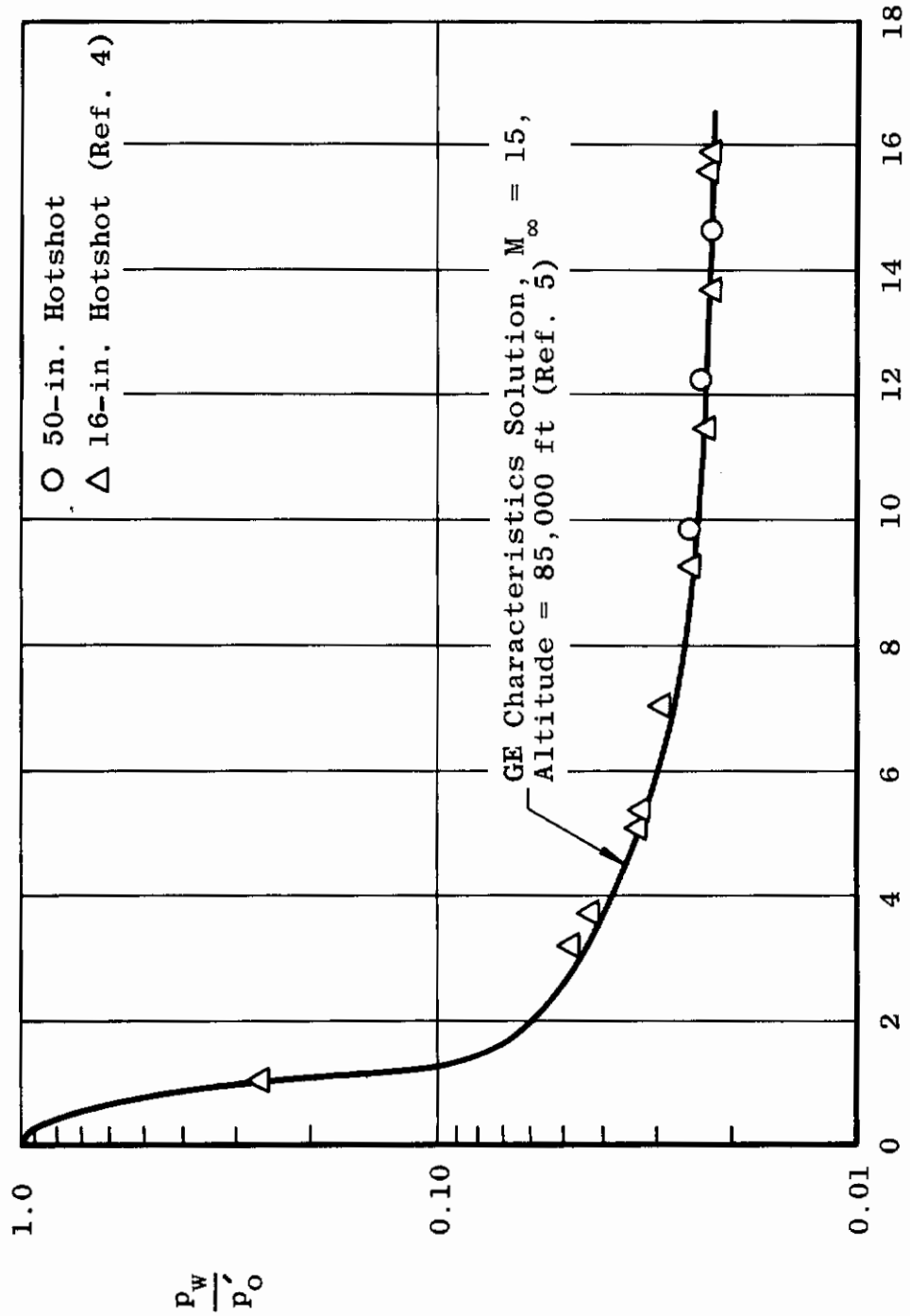

Fig. 8 Pressure Distribution, Spherically Blunted 9-Deg Cone